Electronic Supplementary Information (ESI) for:

Triple-chain Boron Clusters: Lengthening via Phosphorus Doping and Enhancing Stability through {P} by {CH} Substitution

Long Van Duong,[a, e] Nguyen Minh Tam,[b] Amir Karton,*[c] Minh Tho Nguyen*[d, e]

[a] Atomic Molecular and Optical Physics Research Group, Science and Technology Advanced Institute, Van Lang University, Ho Chi Minh City, Vietnam. Email: duongvanlong@vlu.edu.vn; ORCID: 0000-0003-3349-3035

[b] Faculty of Basic Sciences, University of Phan Thiet, 225 Nguyen Thong, Phan Thiet City, Binh Thuan, Vietnam. ORCID: 0000-0003-3153-4606

[c] School of Science and Technology, University of New England, Armidale, NSW 2351, Australia. Email: *amir.karton@une.edu.au,* ORCID: 0000-0002-7981-508X

[d] Laboratory of Chemical Computation and Modeling, Institute for Computational Science and Artificial Intelligence, Van Lang University, Ho Chi Minh City, Vietnam. Email: *minhtho.nguyen@vlu.edu.vn*; ORCID: 0000-0002-3803-0569

[e] Faculty of Applied Technology, School of Technology, Van Lang University, Ho Chi Minh City, Vietnam

Table of Contents

The AdNDP analysis for the T_d $B_{16}P_4$-3 isomer

The AdNDP analysis has been conducted by Gao *et al.*,[1] for the T_d **$B_{16}P_4$-3** isomer, but our present attempt to reproduce their results (Figure S1) does not yield identical results. Initially, we successfully reproduce (1) 4 lone pairs of P atoms with the occupation number of ON = 1.88 |e| and (2) 12 localized (2c-2e) B-P with ON = 1.85 |e|. Next, Gao *et al.* identified 12 (3c-2e) bonds with ON = 1.81 |e|, whereas we observe a larger deviation with ON = 1.76 |e| for these bonds (3). In fact, to achieve a bond pattern similar to that reported by Gao *et al.*, we need to employ a small trick: selecting (4) 6 (4c-4e) bonds before (3) choosing the 12 (3c-2e) bonds. The outcome of these selections leaves 5.38 residual valence electrons across all atoms in the search list. What surprises us is our inability to find any additional bonds from these 5.38 residual valence electrons. If we were to select first the 12 (3c-2e) bonds, their ON would be 1.89 |e|, and we were not unable to locate any (4c-2e) bonds. From this point, we have two alternative options with outcomes as depicted in Figures S1.b and S1.c. The first option, as depicted in Figure S1.b, shows that the (4) 6 (4c-2e) bonds transform into (6) 4 (6c-2e) bonds and (7) 2 (20c-2e) bonds. The second option, illustrated in Figure S1.c, indicates that the (4) 6 (4c-2e) could alternatively be (9), (10), and (11) 6 (20c-2e) bonds, with the shape of these bonds possibly conforming to the electron configuration $1S^2 1P^6 1D^4$. In summary, we present here three ways to interpret chemical bonds in T_d **$B_{16}P_4$-3** isomer based on the adaptive natural density partitioning (AdNDP) approach, but in reality, there may be additional interpretations as AdNDP is inherently a subjective, if not arbitrary, method. The first approach includes the bonds depicted in Figure S1.a. The second approach encompasses bonds (1), (2), and Figure S1.b, while the third involves bonds (1), (2), and Figure S1.c. All three methods essentially indicate that T_d **$B_{16}P_4$-3** isomer actually exhibits relatively low thermodynamic stability. Indeed, the third method seems to provide us with the most accurate description of the chemical bonding in **$B_{16}P_4$-3**, demonstrating that delocalized electrons occupy the $1S^2 1P^6 1D^4$

shells with the D shell remaining incomplete. In the second method, although there are no [$1S^2 1P^6$] shells, bonds within the incomplete D shell still exist. The geometric shape of these D-shape bonds is similar to the HOMO and HOMO' of **$B_{16}P_4$-3**, as depicted in Figure S1.d.

Finally, the first method is reminiscent of the presentation by Gao *et al*., which demonstrated that **$B_{16}P_4$-3** does not possess any global delocalized electrons, even with only (16c-2e) with the center being formed by 16 B atoms. This contradicts the usual stability observed in boron clusters where global delocalized electrons are always present in highly stable clusters.

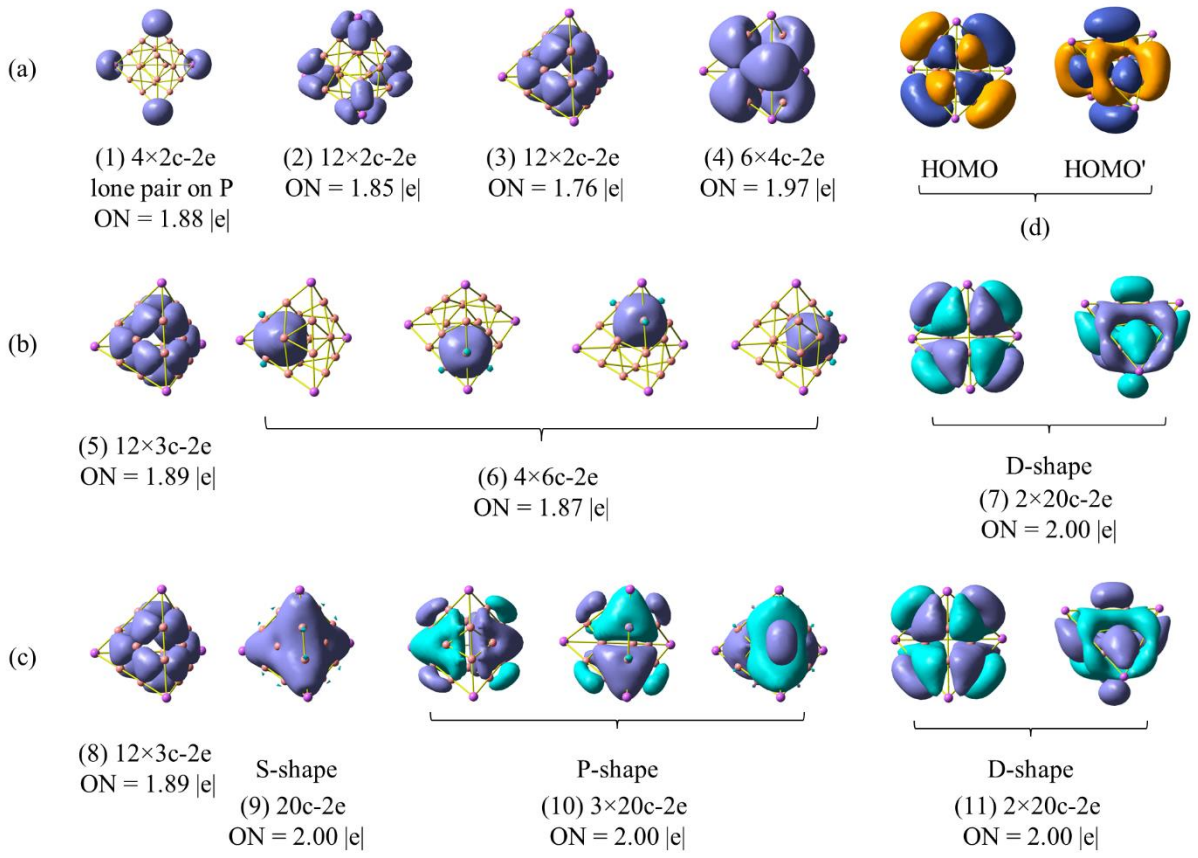

Figure S1. Chemical bond / orbitals pattern of T_d tetrahedron **$B_{16}P_4$-3** isomer on the basis of adaptive natural density partitioning (AdNDP) analysis. Occupation numbers (ONs) are indicated.

1. The anion $B_xP_yC_zH_z^-$

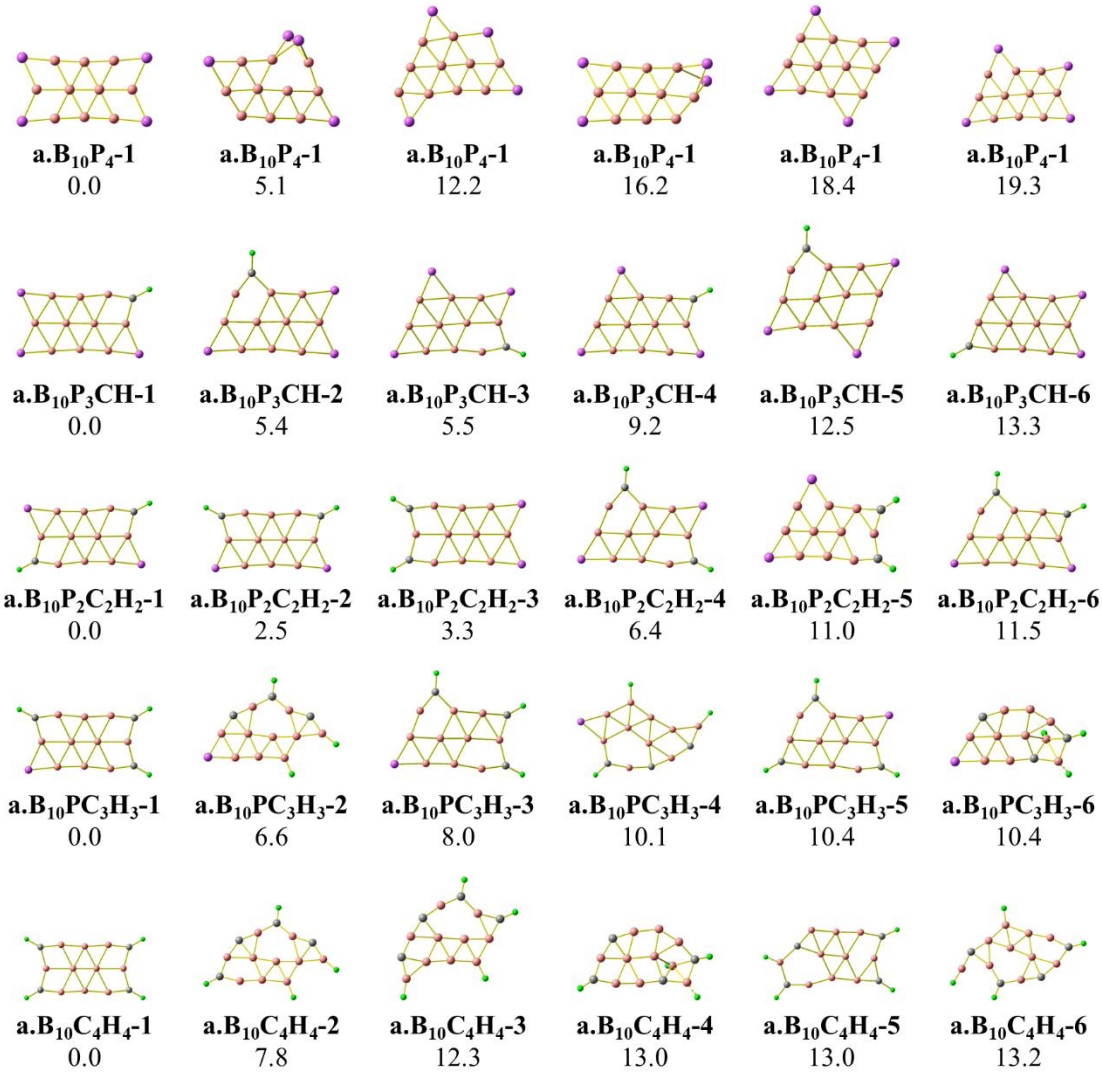

Figure S2. Optimized geometries of the lowest-lying anion $B_{10}P_yC_zH_z^-$ isomers with y = 0 – 4 and z = 4 – y. Relative energies, given in kcal/mol, are obtained from PBE/6-311+G(d) + ZPE values.

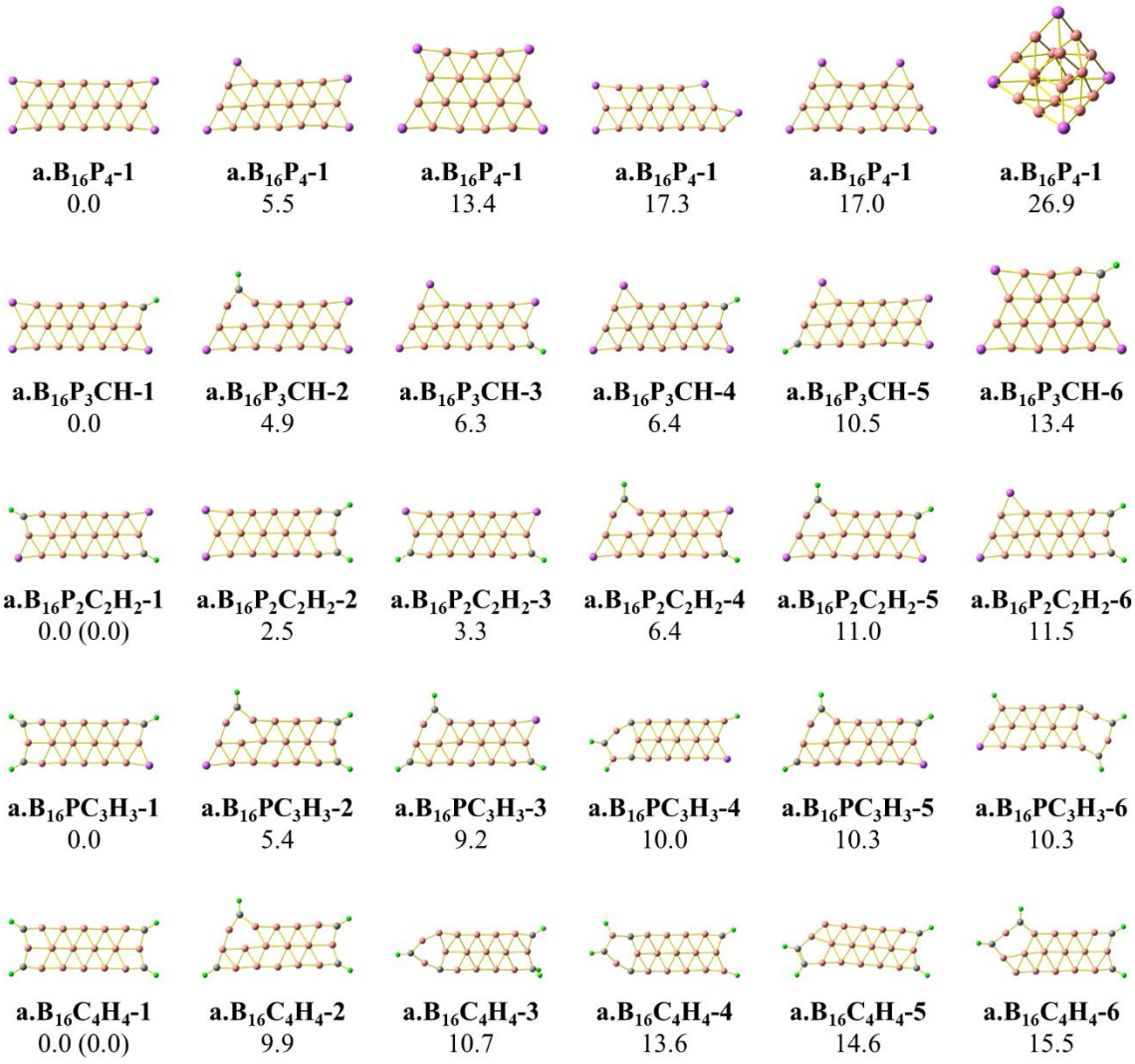

Figure S3. Optimized geometries of the lowest-lying anion $B_{16}P_yC_zH_z^-$ isomers with y = 0 – 4 and z = 4 – y. Relative energies, given in kcal/mol, are obtained from PBE/6-311+G(d) + ZPE values.

2. Chemical bonding

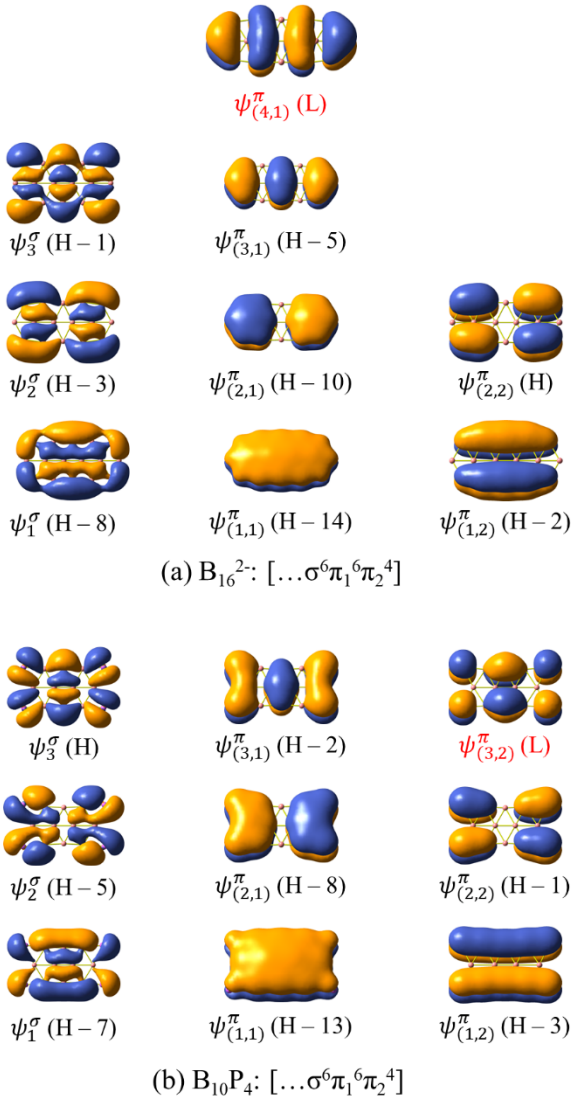

Figure S4. The σ delocalized and π MOs of **(a)** B_{16}^{2-} and **(b)** $B_{10}P_4$. H and L stand for HOMO and LUMO, respectively.

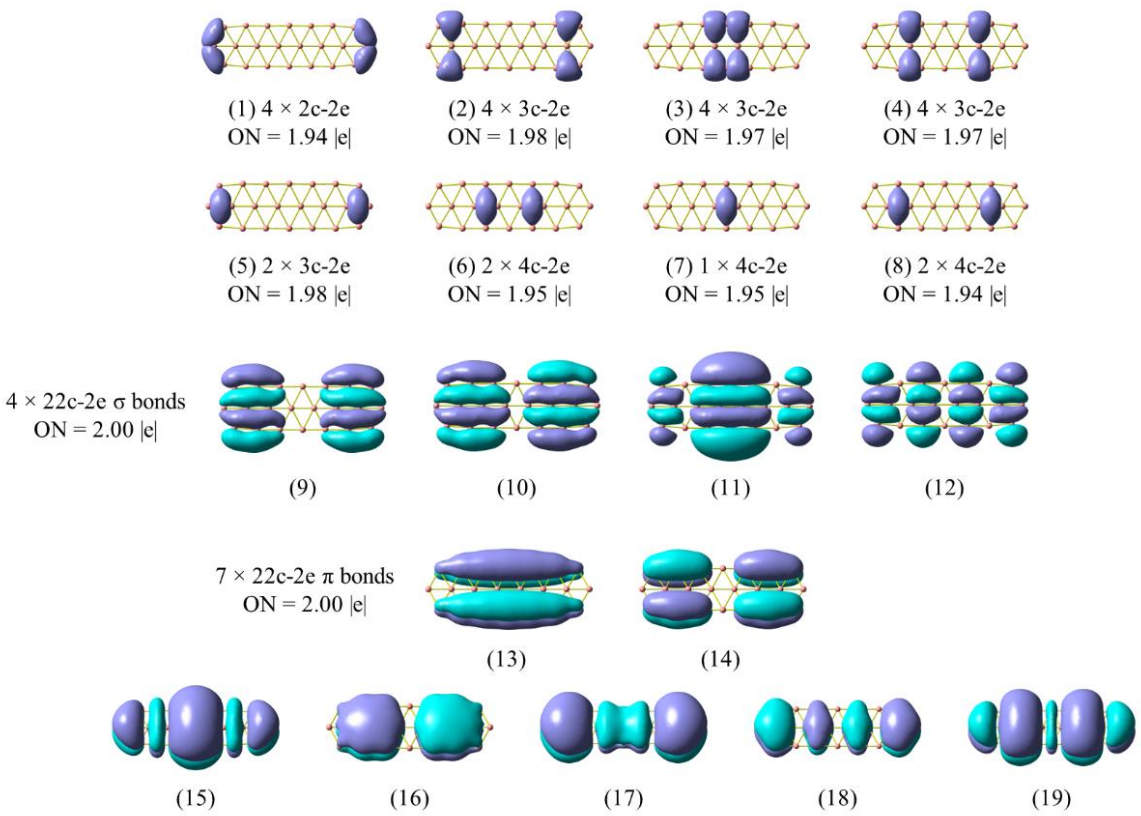

Figure S5. Chemical bonding pattern of B_{22}^{2-} on the basis of AdNDP analysis.

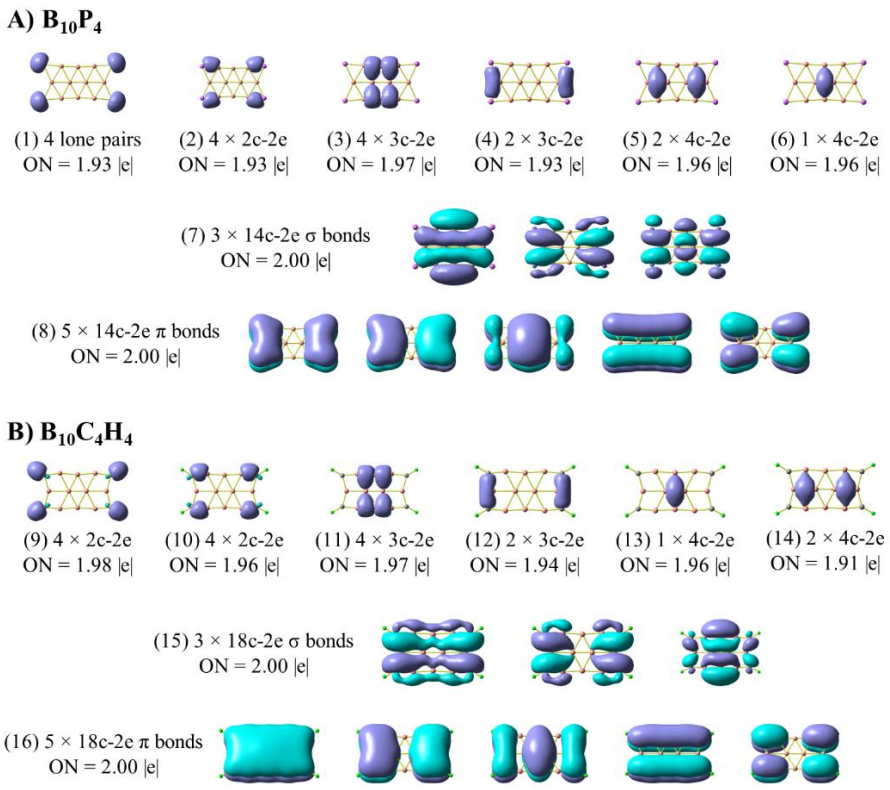

Figure S6. Chemical bonding pattern of **a)** $B_{10}P_4$ and **b)** $B_{10}C_4H_4$ on the basis of AdNDP analysis.

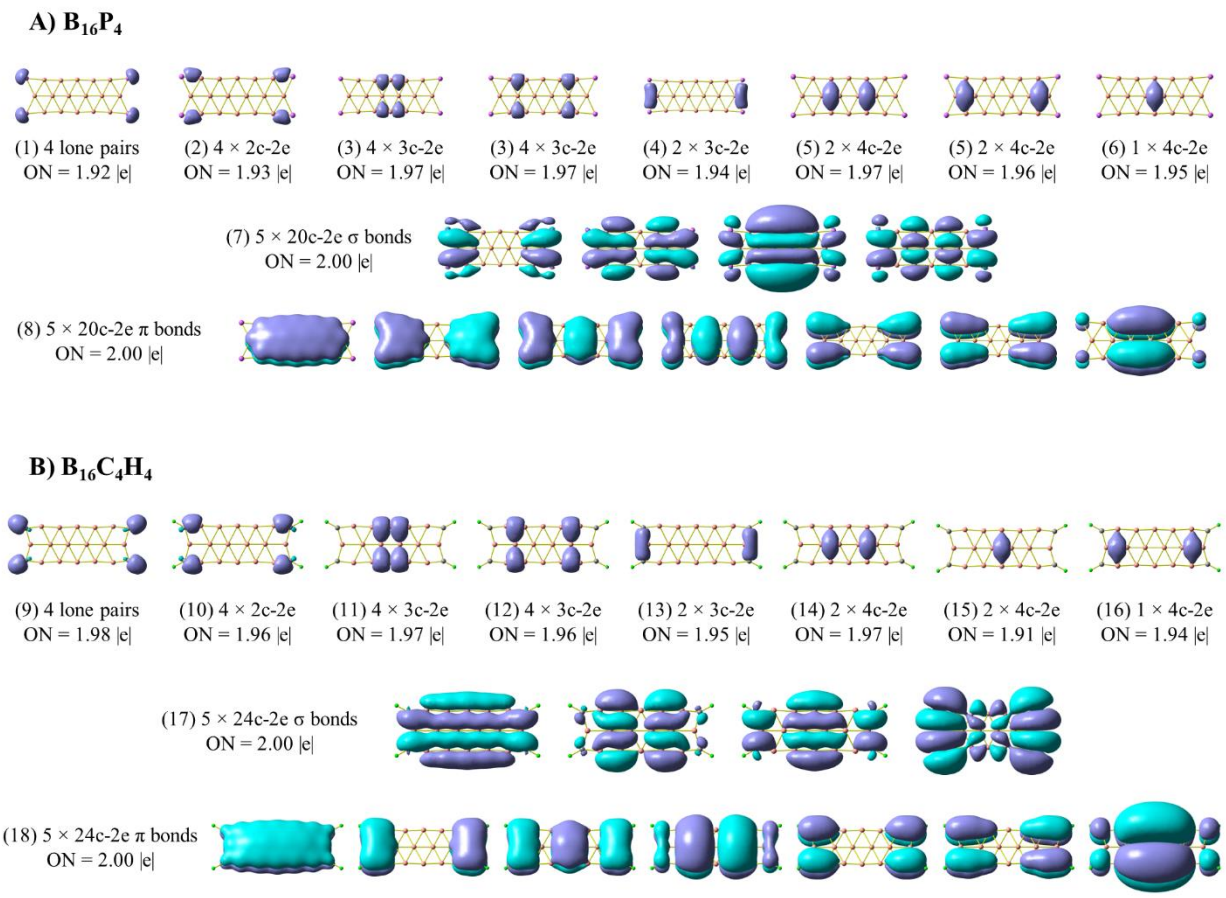

Figure S7. Chemical bonding pattern of **a)** $B_{16}P_4$ and **b)** $B_{16}C_4H_4$ on the basis of AdNDP analysis.

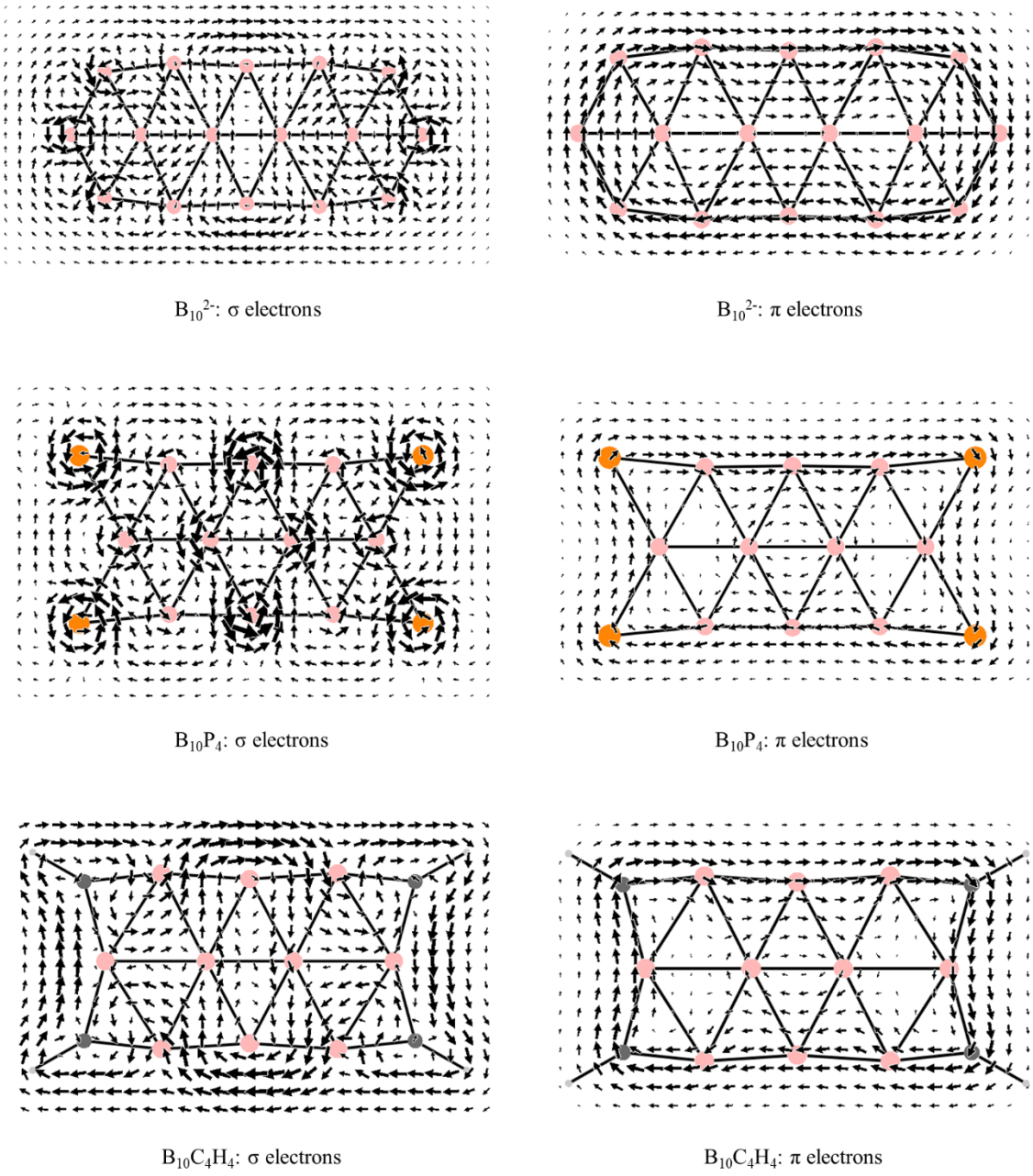

Figure S8. The σ and π magnetic ring current maps of B_{16}^{2-}, $B_{10}P_4$ and $B_{10}C_4H_4$ elongated.

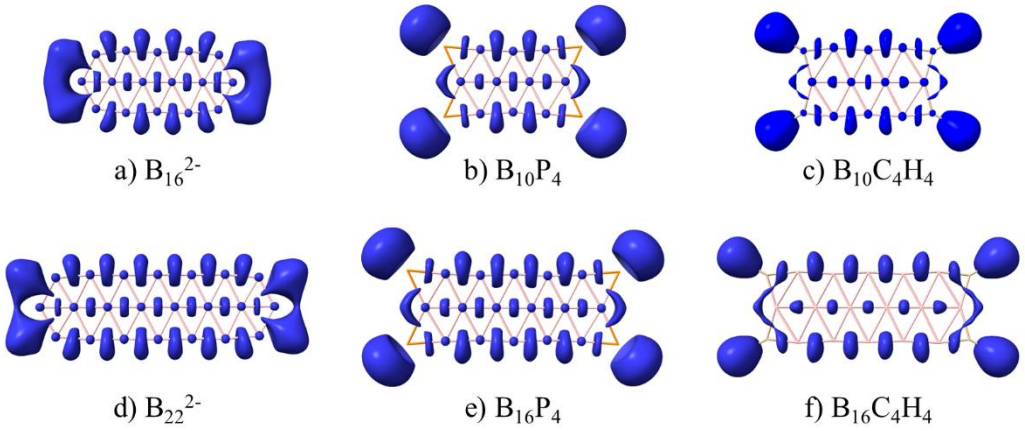

Figure S9. The electron localization function ($ELF_{\sigma l}$) maps of **a)** B_{16}^{2-}, **b)** $B_{10}P_4$, **c)** $B_{10}C_4H_4$, **d)** B_{22}^{2-}, **e)** $B_{16}P_4$, and **f)** $B_{16}C_4H_4$.

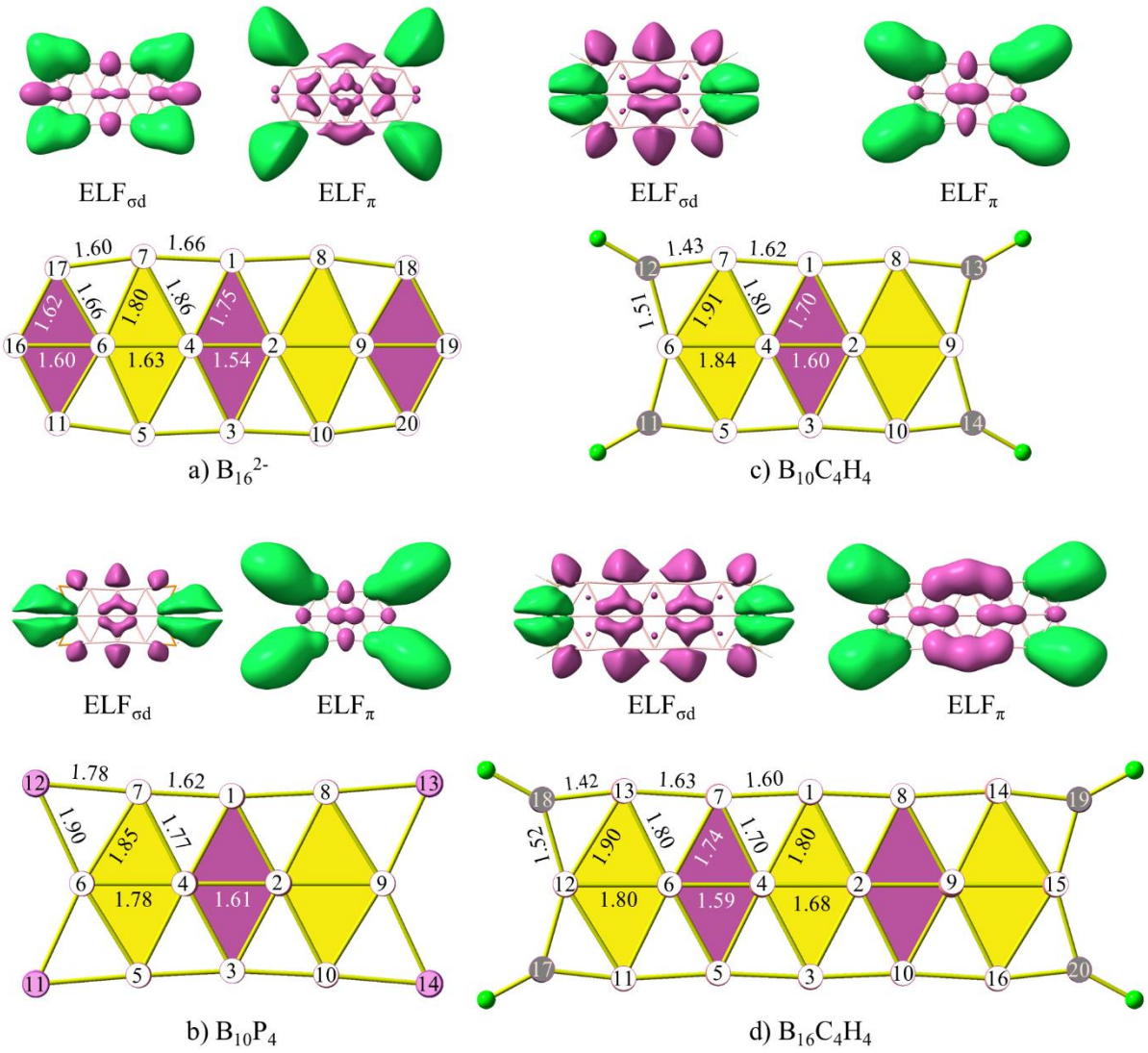

Figure S10. The ELF$_{\sigma d}$, ELF$_{\pi}$, and the structures of **a)** B_{16}^{2-}, **b)** $B_{10}P_4$, **c)** $B_{10}C_4H_4$ and **d)** $B_{16}C_4H_4$. Bond lengths are given in angstrom.

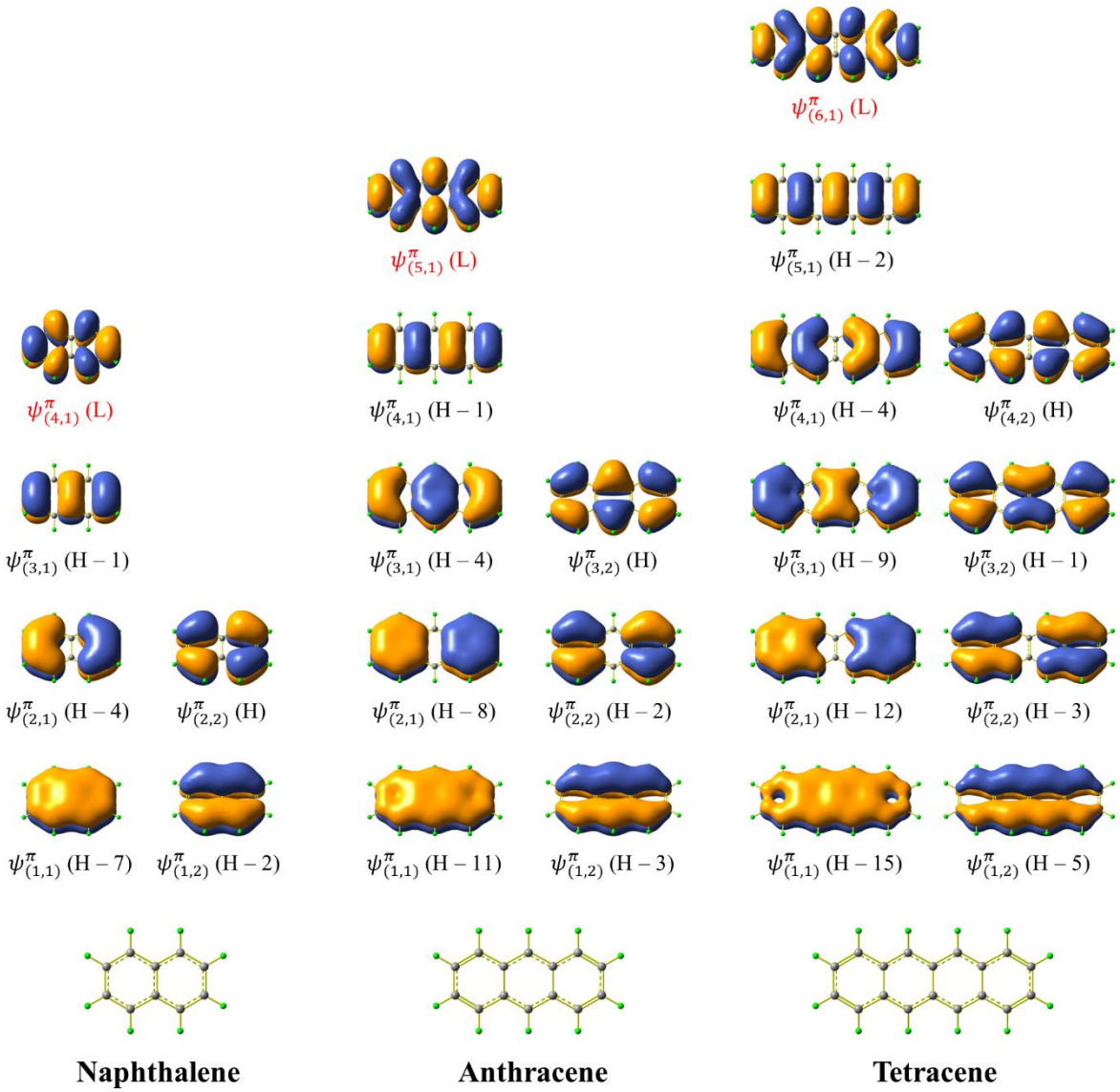

Figure S11. The π MOs of naphthalene, anthracene, and tetracene. H and L stand for HOMO and LUMO, respectively.

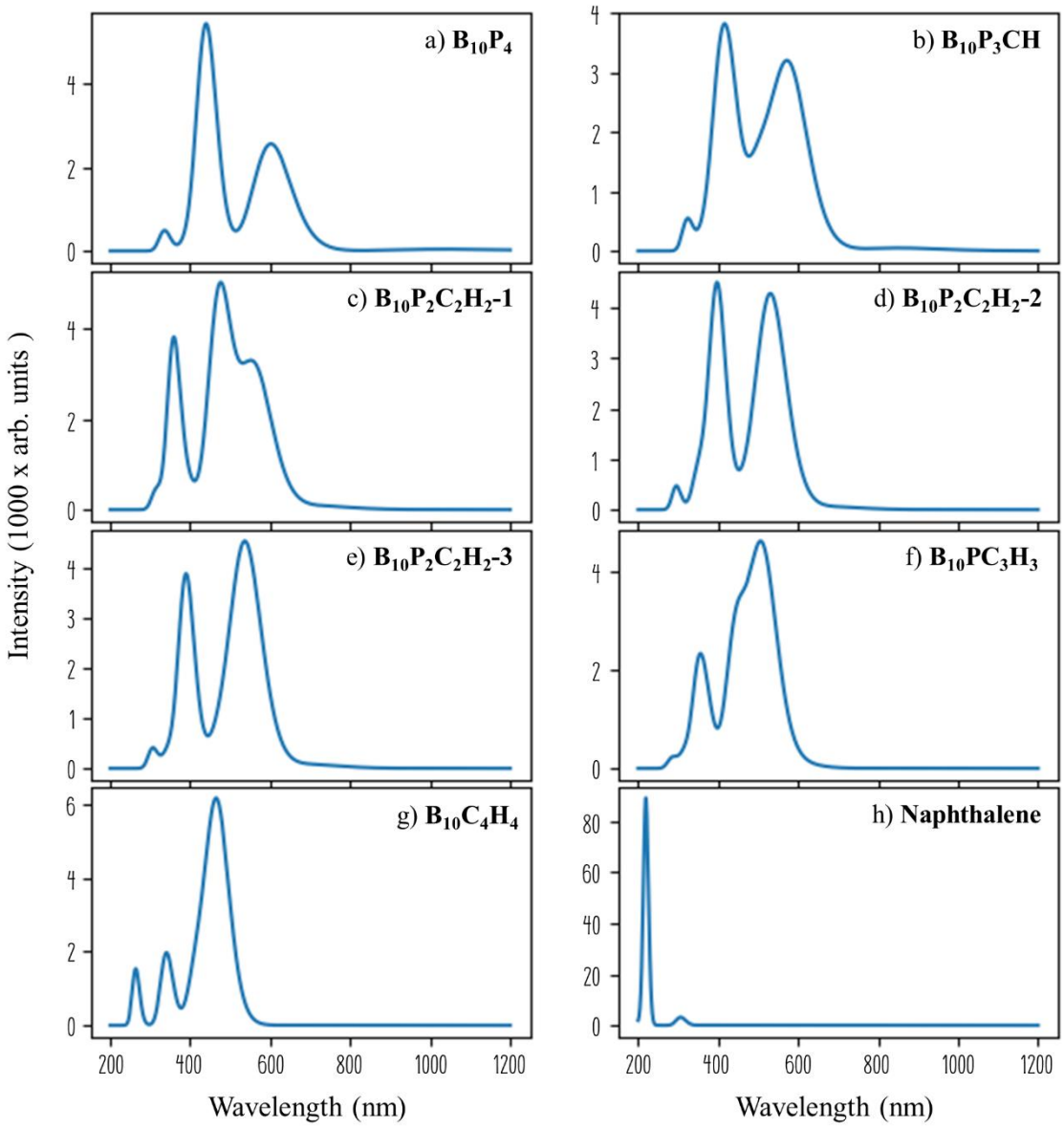

Figure S12. Predicted electronic absorption spectrum of the **a)** $B_{10}P_4$, **b)** $B_{10}P_3CH$, **c)** **$B_{10}P_2C_2H_2$-1**, **d)** **$B_{10}P_2C_2H_2$-2**, **e)** **$B_{10}P_2C_2H_2$-3**, **f)** $B_{10}PC_3H_3$, **g)** $B_{10}C_4H_4$, and **h)** naphthalene ($C_{10}H_8$).

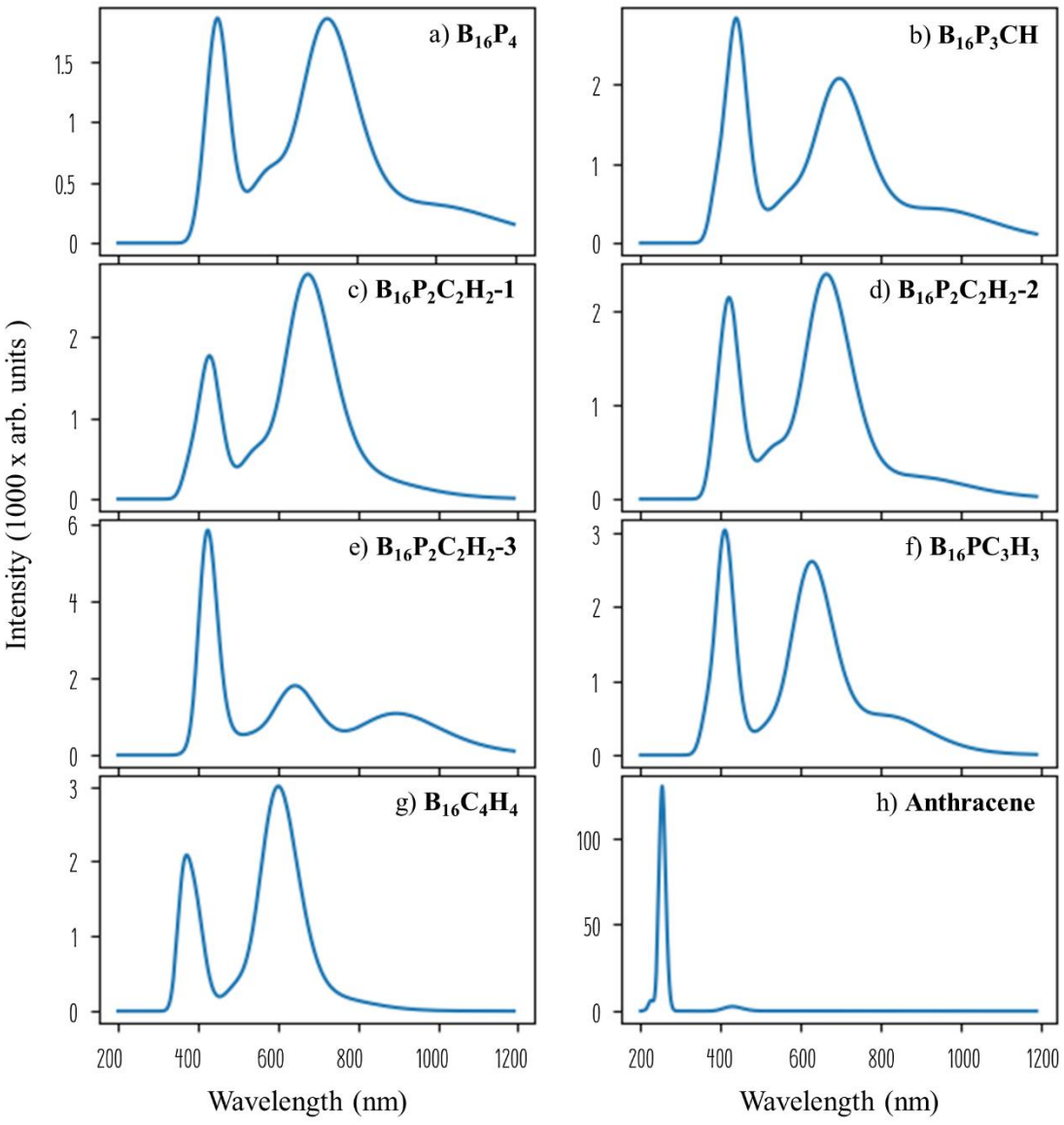

Figure S13. Predicted electronic absorption spectrum of the **a)** $B_{16}P_4$, **b)** $B_{16}P_3CH$, **c)** **$B_{16}P_2C_2H_2$-1**, **d)** **$B_{16}P_2C_2H_2$-2**, **e)** **$B_{16}P_2C_2H_2$-3**, **f)** $B_{16}PC_3H_3$, **g)** $B_{16}C_4H_4$, and **h)** anthracene ($C_{14}H_{10}$).

Table S1. The HOMO – LUMO gap (HLG), VIE, VAE, hardness (η), electronegativity (χ) and electrophilicity (ω) values of $B_{10}P_yC_zH_z$ clusters. All values are in eV.

	HLG	**VAE**	**VIP**	**η**	**χ**	**ω**
B_{10}	1.72	2.51	8.80	3.14	5.66	5.09
$B_{10}P$	0.60	3.10	8.05	2.48	5.57	6.27
$B_{10}P_2$	1.78	2.60	8.47	2.93	5.54	5.23
$B_{10}P_3$	0.56	3.29	7.84	2.28	5.56	6.80
$B_{10}P_4$	1.11	2.88	7.76	2.44	5.32	5.81
$B_{10}P_3CH$	1.37	2.74	7.93	2.60	5.33	5.48
$B_{10}P_2C_2H_2$	1.60	2.61	8.12	2.75	5.36	5.22
$B_{10}PC_3H_3$	1.96	2.34	8.26	2.96	5.30	4.74
$B_{10}C_4H_4$	2.18	2.06	8.25	3.09	5.16	4.30

Table S2. The HOMO – LUMO gap (HLG), VIE, VAE, hardness (η), electronegativity (χ) and electrophilicity (ω) values of $B_{16}P_yC_zH_z$ clusters. All values are in eV.

	HLG	**VAE**	**VIP**	**η**	**χ**	**ω**
B_{16}	1.06	3.01	7.87	2.43	5.44	6.10
$B_{16}P$	0.36	3.53	7.64	2.05	5.58	7.60
$B_{16}P_2$	1.03	3.23	7.81	2.29	5.52	6.66
$B_{16}P_3$	0.38	3.49	7.31	1.91	5.40	7.64
$B_{16}P_4$	0.92	3.28	7.49	2.10	5.39	6.90
$B_{16}P_3CH$	1.06	3.12	7.48	2.18	5.30	6.44
$B_{16}P_2C_2H_2$	1.20	2.91	7.47	2.28	5.19	5.91
$B_{16}PC_3H_3$	1.26	2.73	7.44	2.35	5.09	5.50
$B_{16}C_4H_4$	1.40	2.50	7.41	2.46	4.96	5.00

3. References

1 C.-Y. Gao, Q.-Q. Yan, Q. Chen, Y.-W. Mu and S.-D. Li, *J. Clust. Sci.*, 2024, **35**, 1375–1380.